OAK RIDGE NATIONAL LABORATORY
operated by
UNION CARBIDE CORPORATION
NUCLEAR DIVISION
for the
U.S. ATOMIC ENERGY COMMISSION

ORNL-TM-1892

COPY NO. - 98

DATE - June 16, 1967

Neutron Physics Division

NUCLEAR REACTION CROSS SECTIONS FOR SPACECRAFT SHIELD DESIGN

R. W. Peelle

Spherical shield geometry is adequate for studying the contribution of nuclear reactions to the dose received by spacecraft occupants. Very high energy incident protons produce in the shield an essentially isotropic volume source proportional to the angle-integrated production cross section. Protons with range too short to penetrate the shield produce a yield dependent upon the current into the shield, with the importance of cross sections at a given energy being dependent on the incident spectrum and the inverse of the stopping power. Protons of intermediate energy penetrate the shield and stop in the pilot, and so are important for primary rather than for secondary dose. If the shield is not too thick, the secondary dose inside the cavity is rather independent of position in both the high- and low-incident energy limits. Therefore, calculations can be made for the dose at the center of the sphere, where the secondary flux from an isotropic primary flux is equal to that obtained in a modified straight-ahead approximation for monodirectional primary protons incident on a slab.

Widely available intranuclear cascade-plus-evaporation calculations give secondary nucleon cross sections which agree fairly well with experiments using incident protons. New data is presented to illustrate that the present model has some limited validity even for incident proton energies as low as 20 MeV. Calculational models are not known to have yielded generally valid cross sections for secondary gamma rays or for secondary neutrons from alpha particles.

NOTE

This Work Supported by
NATIONAL AERONAUTICS AND SPACE ADMINISTRATION
Under Order R-104(10)

*Invited paper to be presented at the 1967 Annual Meeting of the American Nuclear Society, San Diego, California, June 11-15, 1967.

TABLE OF CONTENTS

I. THE INFLUENCE OF SPACECRAFT GEOMETRY ON THE RELATIVE IMPORTANCE OF NUCLEAR SECONDARY CROSS SECTIONS

When we wish to think in a simple way about the influence of secondary nuclear radiations on the shield design of a spacecraft, we can think of the cabin as a one-dimensional sphere with the pilot conveniently huddled in the center as illustrated in Fig. 1. The incident protons and alpha particles, averaged over the flight, are assumed to be isotropic in the absence of the vehicle. We are concerned with any influence that nuclear reactions in the shield may have on the dose to the pilot. The shield is thin enough, in terms of the interaction length of the secondary neutrons and gamma rays, that multiple collisions cannot dominate. We are also concerned with how the reactions of primary (or secondary) particles in the pilot may affect him. This discussion aims to help clarify which cross sections are important.

The sphere geometry seems crude, but it is adequate for the present purpose. The broad angular distribution of secondary radiations allows us a simple shield representation even for cases that seem to demand great geometric complexity for estimation of the dose from degraded primaries. If we ever become ready to abandon our sphere, at worst only a few simply shaped shield regions will be needed. (Pathlengths through the various gross regions may be preserved from primary dose calculations to allow good secondary source strength estimations.) On the other hand, precise nuclear calculations will be needed for the simpler geometries so that we will not be misguided about complex multiple-collision effects or the influence of detailed spectra.

ORNL-DWG 67-5871

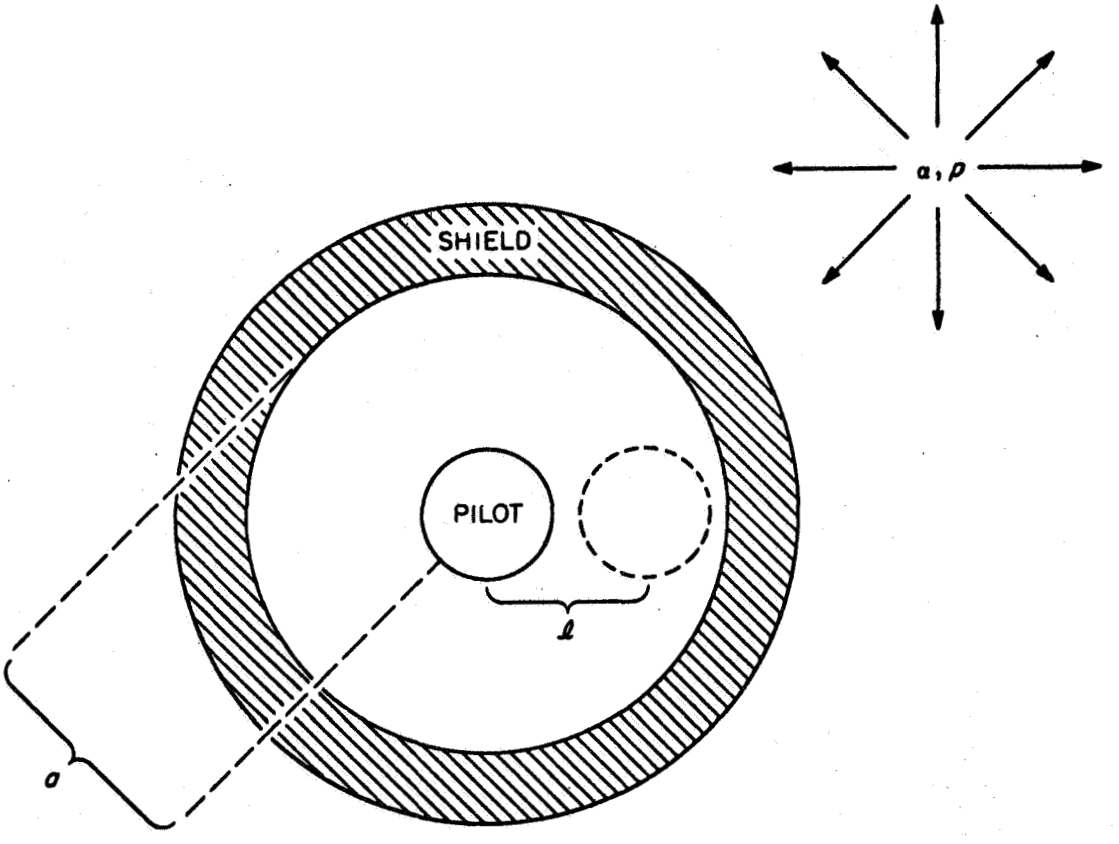

Fig. 1. An Adequate Geometry to Represent a Spacecraft Cabin for Studying the Effects of Nuclear Secondaries.

How can we decide whether a primary proton of given energy E will damage the pilot directly or by way of secondary particles? The relation of shield thickness to incident-particle range distinguishes three cases:

a) Primaries so energetic that they pass completely through the cabin and its occupants lose little enough energy in their continuous slowing-down process that secondary reactions can well compete. The slow energy dependence of the relevant cross sections implies that there is produced in this case an isotropic volume source of secondaries throughout the shield, independent of the angle variations of the differential cross sections. Ignoring details of secondary particle type and energy spectrum, the strength (cm^{-3}) of this volume source V is

$$V = \int_{E_a}^{\infty} \Phi(E)\, \Sigma(E)\, dE \quad , \tag{1}$$

where $\Phi(E)$ is the incident flux integrated over all solid angle, and Σ is the macroscopic cross section at energy E for production of the secondaries being considered. Σ includes the multiplicity.

b) Less energetic primaries which penetrate the shield but stop in the pilot contribute the dominant share of the primary dose, so secondaries in this case are relatively unimportant. (For a 5-g/cm^2 shield we are talking about proton energies between 70 and 200 MeV). For simplified calculations the temptation should be overwhelming to treat secondary production by these primaries as if Eq. (1) were valid.

c) Low-energy charged primaries cannot penetrate the shield, but their secondary neutrons and gamma rays can. The current of low-energy particles into the spacecraft skin produces a surface secondary source of strength

S (cm^{-2}) given by

$$S = \frac{1}{4}\int_0^{E_c} dE' \, \Phi(E') \int_0^{E'} \frac{\Sigma(E)\, dE}{|dE/dx|} \quad . \tag{2}$$

The stopping power enters in the denominator because to find the yield one must integrate over the path of each primary from its original energy down to zero. Unlike the volume source produced by the high-energy primaries, the surface source strength usually has an angular distribution relative to the shield normal. Equation (2) is in the proper form if input data is to be cast as thick-target yields for stopping a primary of energy E'. The order of integration is reversed to employ the cross section at a given energy and the integral flux $\Delta\Phi^i(E)$ up to the cutoff E_c at which the range equals the shield thickness; that is,

$$\begin{aligned} S &= \frac{1}{4}\int_0^{E_c} \frac{dE\, \Sigma(E)}{|dE/dx|} \int_E^{E_c} \Phi(E')\, dE' \\ &= \frac{1}{4}\int_0^{E_c} \frac{dE\, \Sigma(E)\, \Delta\Phi^i(E)}{|dE/dx|} \quad . \end{aligned} \tag{2a}$$

I think that plausible assessment of the importance of this surface source of gamma rays and neutrons is the most obviously unsolved problem in space shielding. We can already say something in the case of gamma rays. Integrated preliminary data of Zobel, Maienschein, and Scroggs [1] suggest that the gamma-ray production cross section for incident protons on aluminum behaves with energy between 15 and 150 MeV almost like the proton stopping power, allowing a quick estimation of the secondary surface source using Eq. (2). The result is that the surface source of gamma rays produced

in aluminum would be about 2×10^{-3} times the incident proton energy current into the shield (less ~15 MeV/proton). With flare spectra which are quite soft, i.e., for a rigidity parameter less than 50 megavolts, it appears that the gamma rays might contribute significantly for shields greater than 10 g/cm^2 thick. For harder flare spectra, aluminum gamma rays cannot produce a significant contribution. Neutron production cross sections behave differently with energy, so a less stringent rule probably applies.

Now let us return to our sphere model. You may question whether it was fair for me to draw the man in the center. Does the sphere integrate so well that this is a good approximation? I have in Fig. 2 a rough answer for the case of an isotropic volume source within the shield. The secondary flux at a point in the interior is estimated as a function of radial position for a sphere 5% as thick as its radius ($t/a = 0.05$). With no attenuation of secondaries the flux rises with radius to 20% above the central value at 2/3 the capsule radius and to about 55% above at 0.9. As secondary attenuation (no scattering) is introduced to the extent of $\Sigma_s t$ mean free paths along the radial direction, the distribution becomes flatter. For present purposes it seems just barely fair to call the central point representative. At the sphere center the secondary flux is

$$F = Vt[1 - \exp(-\Sigma_s t)]/\Sigma_s t \quad . \qquad (3)$$

Equation (3) reduces to $F = Vt$ for small $\Sigma_s t$, and to $F = V/\Sigma_s$ for large $\Sigma_s t$. This is the same estimate one would obtain in the straightahead approximation! As stated by Wallace et al.,[2] the straightahead approximation for the spherical shell in an isotropic flux, viewed at the sphere center, gives the same numerical result as the same approximation gives for a slab of

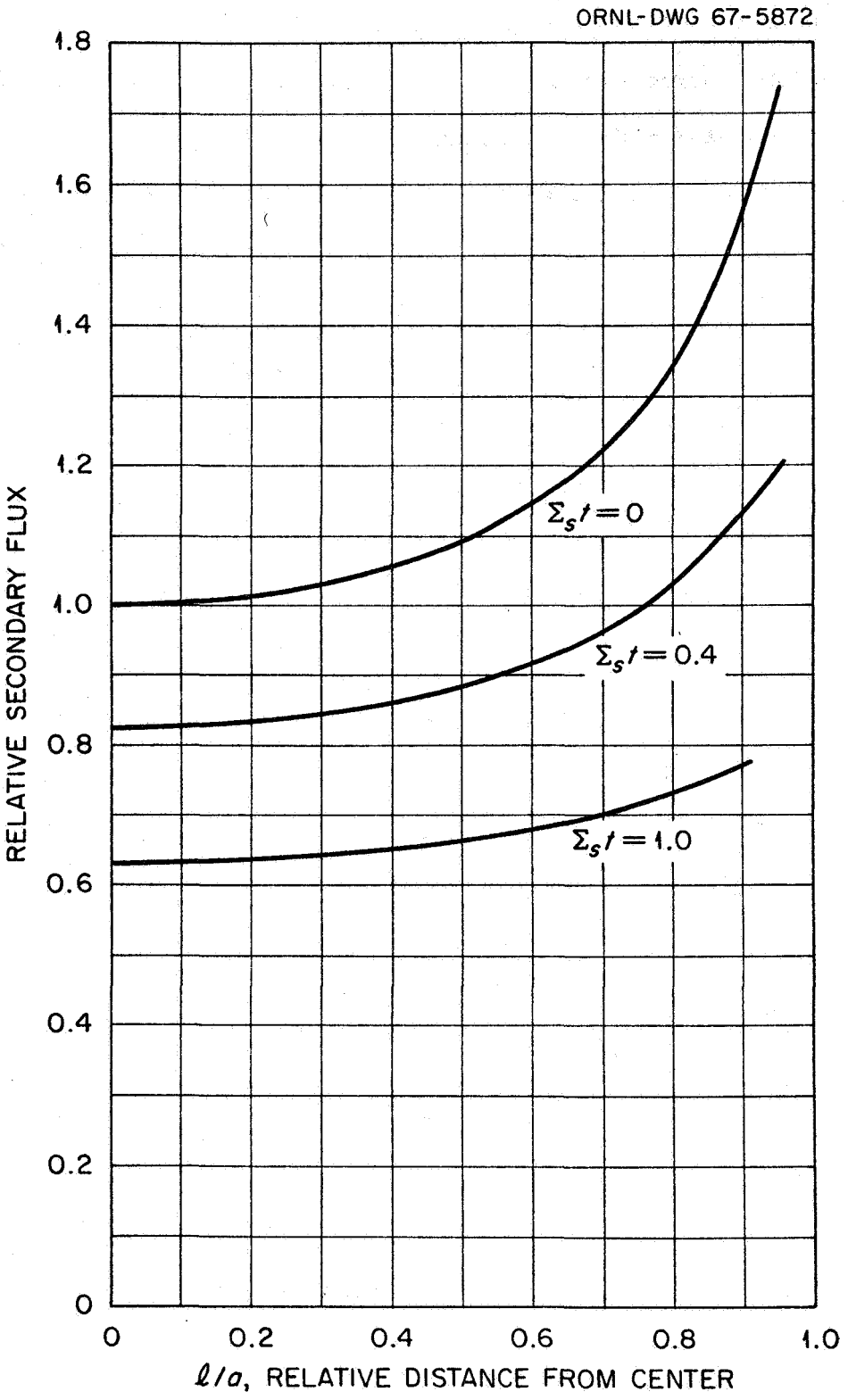

Fig. 2. Interior Flux vs. Radial Position for a Spherical Shell Volume Source of Thickness t Equal to 5% of the Radius. Σ_s is the macroscopic cross section for the secondary radiation.

the same thickness with normally incident (not isotropic) flux. Recall that the volume source strength V has an energy spectrum but contains only the angle-integrated differential cross sections.

A similar approach was made to the problem of secondaries from the low-energy primaries which cannot penetrate the shield. The current rather than the flux is important, so the surface source strength is a function of angle unless the cross sections for secondary production are isotropic. Using the (assumed isotropic) integral primary flux $\Delta\Phi^i$ defined in Eq. (2a), the contribution to the angle-differential surface source strength (cm^{-2} sr^{-1} MeV^{-1}) from the differential macroscopic cross sections $\Sigma(E,\alpha)$ is

$$S(E,\Psi) = \frac{\Delta\Phi^i(E)}{4\pi|dE/dx|}\int_\Omega d\Omega \cos\beta\, \Sigma(E,\alpha) \quad , \tag{4}$$

where β and Ψ are respectively the angles relative to the shield normal of the primary and secondary particles, and α is the angle between the two particles. For a detector at the center of the sphere, $\Psi = 0$ and $\beta = \alpha$, and the angular distributions as expected occur weighted by the cosine of the scattering angle. When the differential cross section is expressed in a Legendre expansion with coefficients $\Sigma_\ell(E)$, i.e.,

$$\Sigma(E,\alpha) = \frac{1}{4\pi}\sum_\ell \Sigma_\ell(E)\, P_\ell(\cos\alpha) \quad , \tag{5}$$

the integral in Eq. (5) may be performed to give the differential surface source:

$$S(E,\Psi) = \frac{\Delta\Phi^i(E)}{16\pi|dE/dx|}\sum_\ell A_\ell\, \Sigma_\ell(E)\, P_\ell(\cos\Psi) \quad . \tag{6}$$

The A_ℓ's may be obtained by applying the addition theorem for spherical harmonics to Eq. (4) using the expansion (5). The resulting integral is known,[3] leading to the results tabulated below.

ℓ	A_ℓ	ℓ	A_ℓ
0	1	3,5,7,...	0
1	2/3	4	-1/24
2	1/4	6	1/192

$$A_\ell = \pi^{1/2}\left[4\Gamma\left(\frac{3-\ell}{2}\right)\Gamma\left(\frac{5+\ell}{2}\right)\right]^{-1}$$

The expression (6) for $S(E,\Psi)$ leads to prediction of the radial dependence of the secondary flux within the cavity, illustrated in Fig. 3. Again it seems provisionally adequate to confine attention to the center of the sphere. If we ignore the detail that all secondaries are not produced just on the skin, the flux at the center is given by

$$F = 4\pi\, e^{-\Sigma_s t}\int_0^{E_c} S(E,0)\,dE$$

$$= \frac{\exp(-\Sigma_s t)}{4}\sum_\ell A_\ell \int_0^{E_c} \frac{\Sigma_\ell(E)}{|dE/dx|}\,\Delta\Phi^i(E)\,dE \quad . \qquad (7)$$

This is the result which would be given by the straightahead approximation using modified production cross sections equal to $\frac{1}{4}\sum_\ell A_\ell\Sigma_\ell$ rather than the

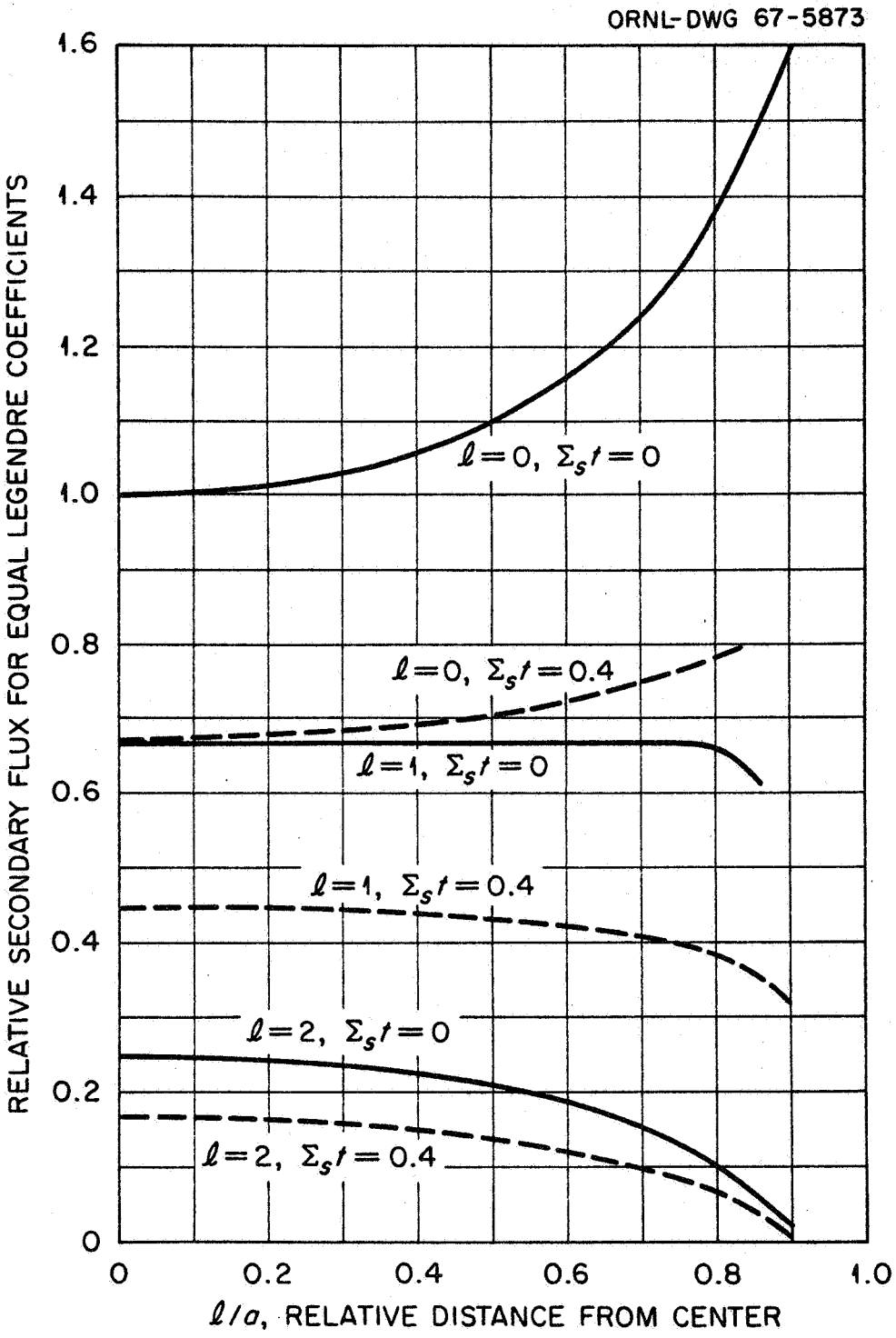

Fig. 3. Interior Flux as a Function of Radius for a Spherical Surface Source Produced by Secondaries from Stopped Charged Particles. The contributions from the first three Legendre coefficients of the differential yield are shown for two values of the normal attenuation thickness $\Sigma_s t$.

customary Σ_0. Again this time, by using the modified cross section, the spherical problem may be adequately transformed to a slab problem with normally incident flux.[b]

To summarize, it appears that our cabin can revert from sphere to slab, that high-energy cross sections are important in a form integrated over angle and weighted by the differential primary flux, and that low-energy cross sections are important integrated over angle, with roughly a $\cos\alpha$ weighting, and weighted by the integral flux over the stopping power.

II. CROSS SECTIONS FOR SECONDARY NUCLEON PRODUCTION

Now consider what knowledge of nuclear cross sections has been made readily applicable to shield design. Generally, it seems preferable to use computed cross sections or interpolations among them, since experiments have not produced results at sufficiently regular energy and angle intervals. This approach is now workable for neutrons (or protons) produced by incident protons from at least 800 MeV down to some nebulous threshold below 100 MeV. By contrast, there is yet little valid guidance from calculations on how to handle neutrons produced by alpha particles.

Every serious shielding effort I have read tries to use nucleon-nucleus cross sections based upon the intranuclear cascade model results of

---

[b] Those who have codes in slab geometry which operate with isotropic incident fluxes and which already contain information on the energy spectra of secondary particles may wish to consider use of the normal emission approximation, in which all secondaries penetrate the shield along the shortest path. This approximation does fairly well conceptually in the high-energy limit, and at low energies yields the appropriate result without the use of modified cross sections. (Isotropic flux on a slab does not transform properly for the primary flux, however.)

Metropolis et al.[4] or the more recent ones of Bertini et al.,[5] though several other similar computations have been made. Bertini's are now available in fitted form[6] and on magnetic tape.[7] These Monte Carlo estimation procedures are based on the idea that, for incident nucleons above perhaps 100 MeV, interactions with the nucleus are dominated by sequential microscopic two-body nucleon-nucleon scattering events for which free-particle cross sections apply. The resulting estimated cross sections are slow functions of angle, incident energy, and target mass, as are experimentally observed cross sections. Figure 4 shows sample differential cross sections at 10, 30, and 45 deg for 160-MeV protons on aluminum. The broad peak at the high-energy end of each spectrum moves with angle almost as it would for billiard-ball cross sections. This peak is a reflection of the use of free-particle kinematics for the microevents, blurred by the momentum distribution assigned to target nucleons and by the occurrence of intranuclear cascades. I have superposed a predicted cross section for Bi at 160 MeV and an appropriately scaled one for Fe at 60 MeV to show how invariant is the predicted differential cross section.

Each intranuclear cascade Monte Carlo history is terminated when no particle has enough energy inside the model nuclear potential to leave the nucleus with more than a specified (low) cutoff energy. The residual excitation energy can be very large; for example, the average excitation energy ranges from 35 to 110 MeV for incident 50- to 400-MeV nucleons on a heavy nucleus like tantalum. This excitation energy is usually handled by assuming that nucleons and heavier fragments "boil off" in variable evaporation chain processes similar to that described and programmed in Monte Carlo by Dostrovsky et al.[8] This evaporation process produces a high (presumably) isotropic contribution at low energies which is not

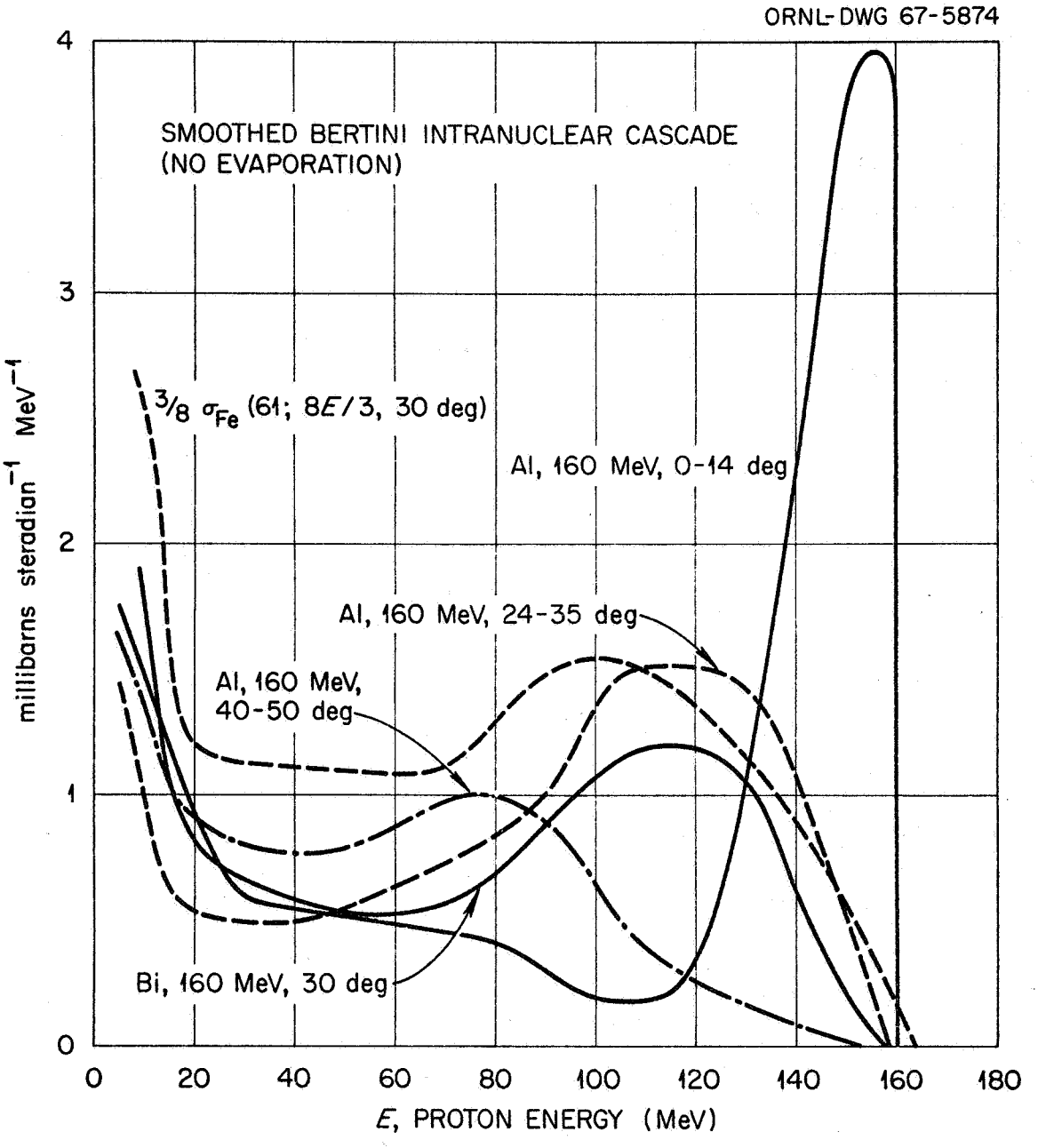

Fig. 4. Hand-Smoothed Differential Cross Sections from the Bertini Intranuclear Cascade Calculation. The cross section for 61-MeV protons on iron has been stretched to preserve constant area.

included in Fig. 4. Estimated cross sections for neutrons look very similar to this figure except that the predicted (largely unmeasured) quasifree scattering peaks are less pronounced, and except that for heavy elements the predicted evaporation yields are quite high.

How valid are the cross sections obtained from the cascade model? They are remarkably so, though as an experimentalist I enjoy dwelling on residual difficulties. For instance, though the works of Wall and Roos[9] and of Genin et al.[10] support the marked quasifree peak in the 45 deg region, our work,[11] the recent results of Brun et al.,[12] and perhaps the 185-MeV data of Dahlgren[13] all tend to require that quasifree scattering be less apparent. Figure 5 shows that at 60 deg Bertini predicts cross sections for 160-MeV protons on Al which are in accord (on an absolute basis, no free parameters) with the experiments of Wachter et al.[14] and myself[11] but not quite with those of Roos and Wall.[9] Neutrons from 140-MeV protons have been studied by Bowen[15] at forward angles, where they characteristically disagree with calculation in the manner shown in Fig. 6; the predicted peak is always too intense and the tail too weak, though the situation does vary a little with target mass number. For a comparison at higher energy, Bertini has recently shown results from a new program which includes meson production.[16] Figure 7 compares his estimates for 660-MeV protons on Cu with the experiment of Azhgirey et al.[17] The new code is final but the cross-section parameters are yet subject to improvement.

Since I have emphasized cross sections integrated over angle, I would like to encourage comparisons on that basis. Figure 8, from the Orsay work of Brun et al.,[12] illustrates that cascade calculations can give fits within 20% to angle-integrated spectra for 156-MeV protons on silver.

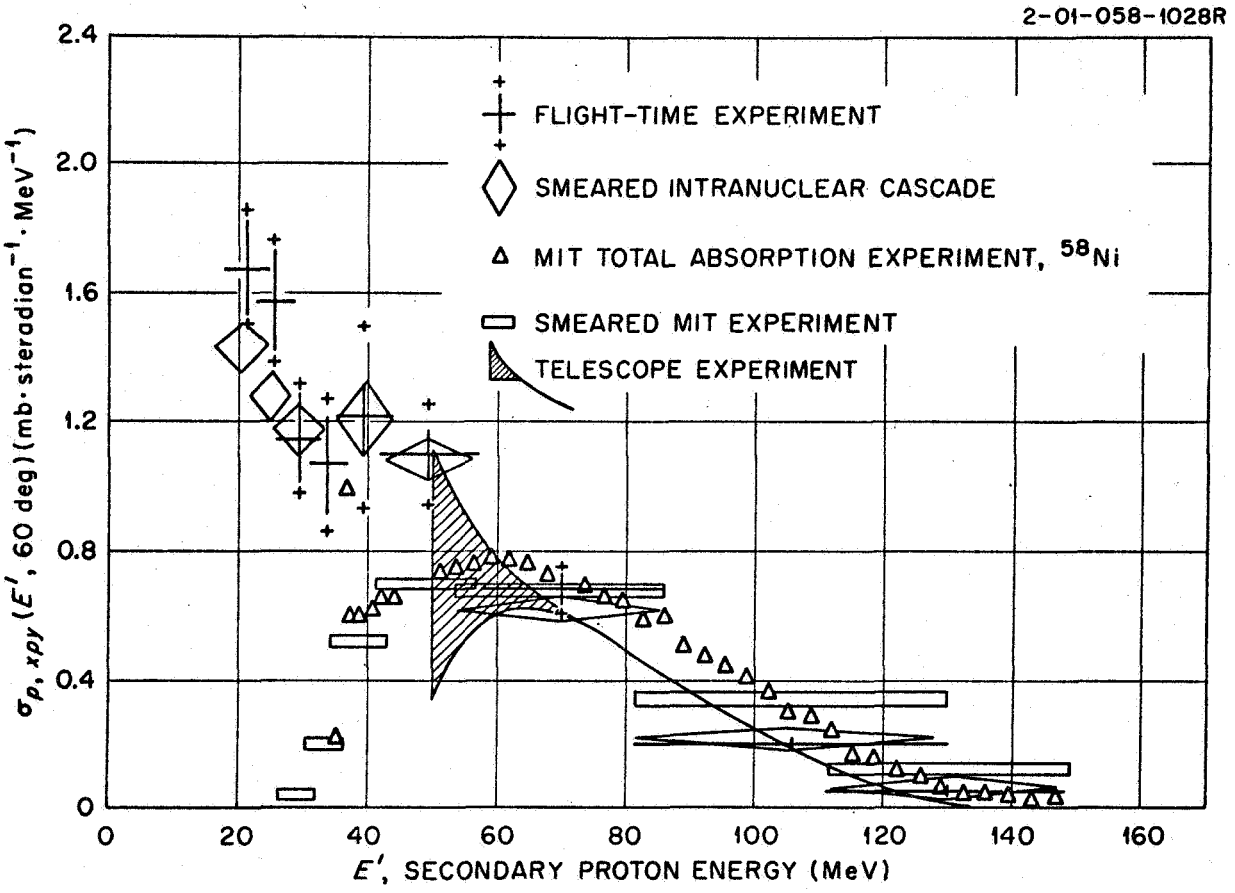

Fig. 5. Differential Cross Sections at 60 deg from 160-MeV Protons on Cobalt. Results from the Bertini calculations and from the MIT experiment of Wall and Roos are shown with and without smearing appropriate to the author's flight-time experiment.

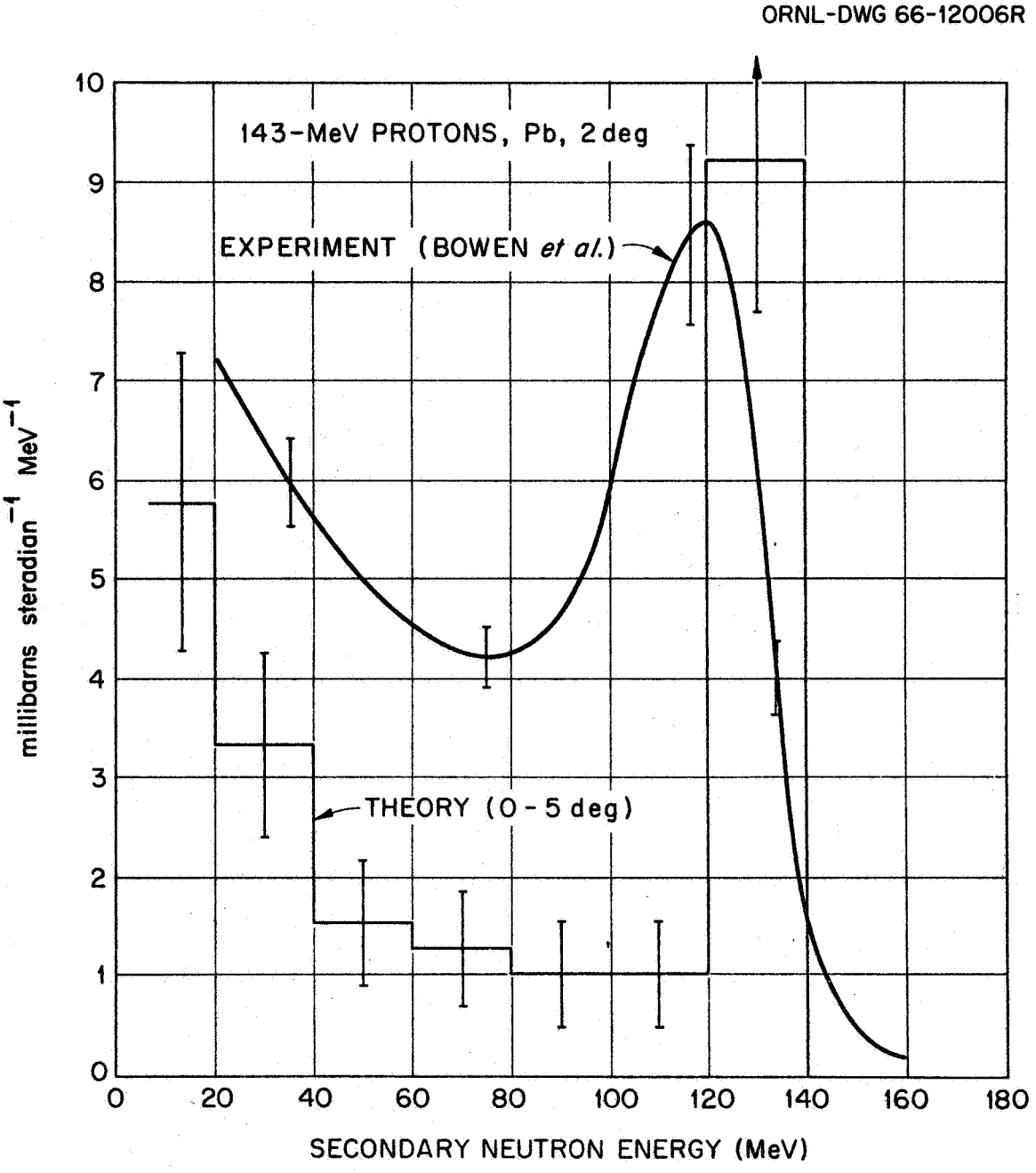

Fig. 6. Comparison of the Bertini Intranuclear Cascade Calculation Against Experiment for Secondary Neutrons at 2 deg from 143-MeV Protons on Lead.

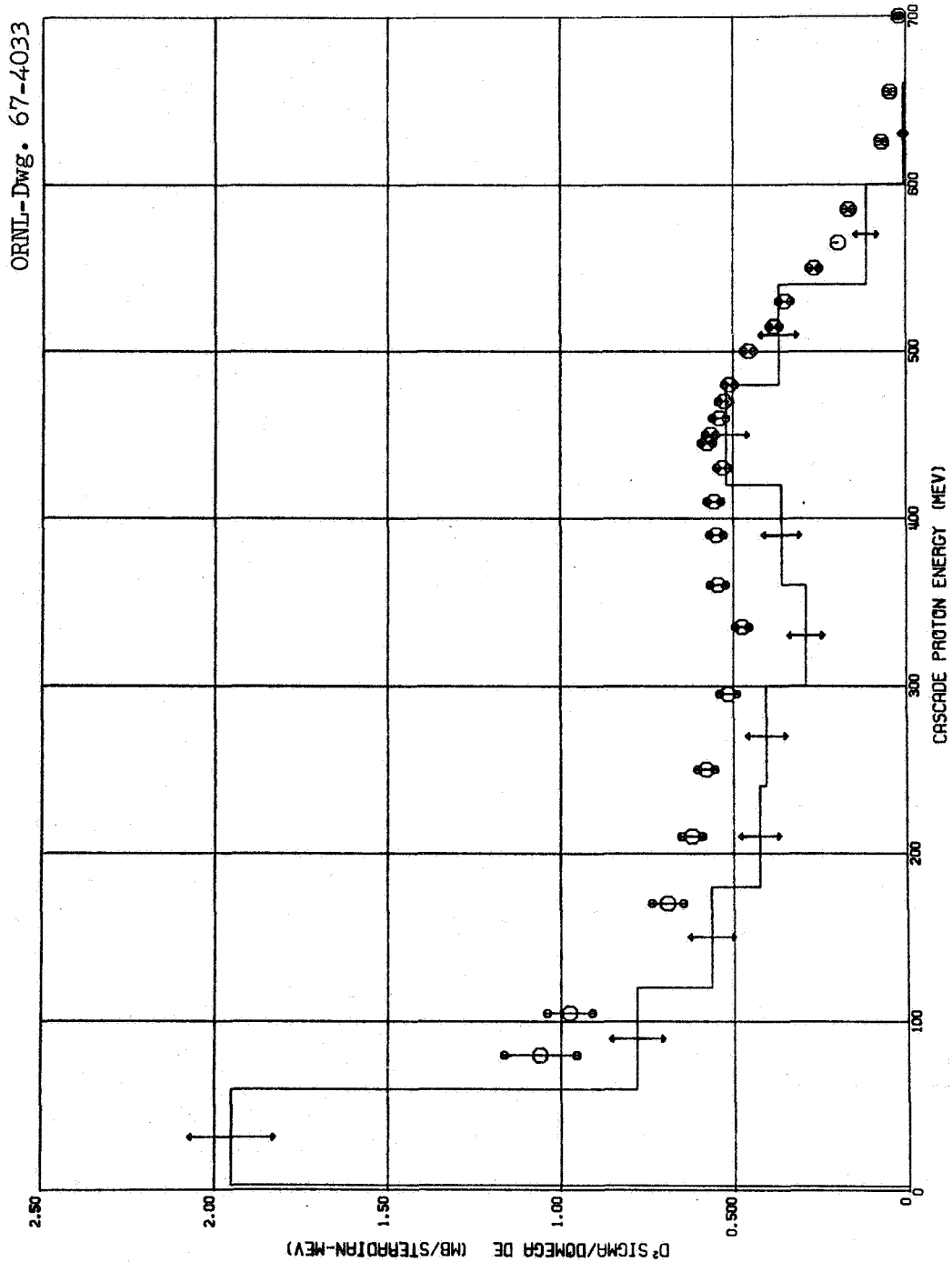

Fig. 7. Secondary Protons at 30 deg from 660-MeV Protons on ^{65}Cu. The high-energy intranuclear cascade predictions of Bertini are compared against the experiment of Azhgirey et al.

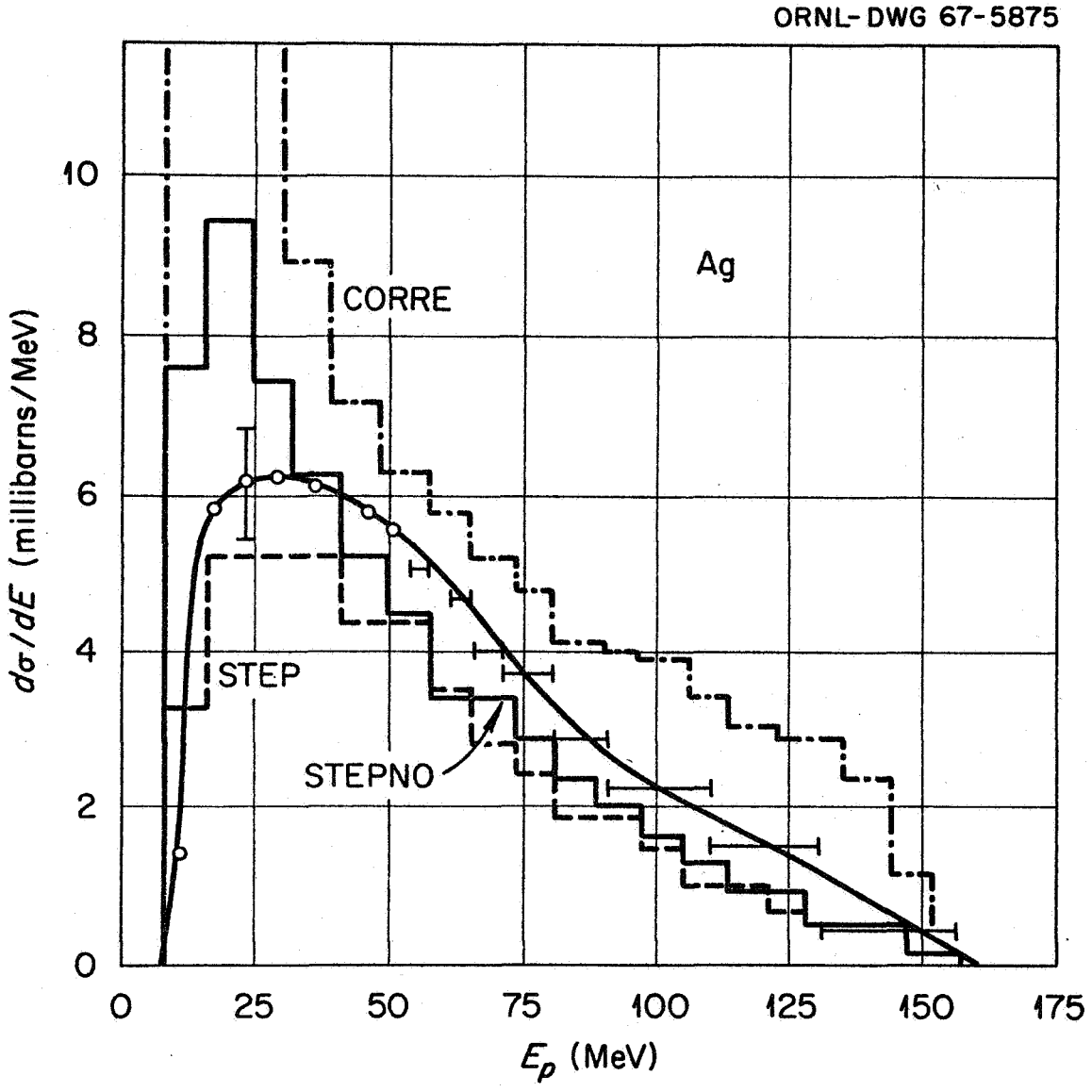

Fig. 8. A Comparison from C. Brun et al. for the Angle-Integrated "Direct Reaction" Proton Spectrum from 156-MeV Protons on Silver. Protons believed to have originated from nucleon evaporation have been subtracted prior to comparison against his three intranuclear cascade calculations. (Courtesy Nuclear Physics.)

The cascade model was originally intended for use with rather high incident energies. What should be used for calculations on the soft flares which are apt to be important for secondary production? Figure 9 shows some recent data of Bertrand et al.[18] at 30 deg for incident 60-MeV protons on ^{54}Fe. Below the region of marked group structure the Bertini model fits well, except that the evaporation proton yield from the associated treatment of nucleon evaporation is twice too large. (I refuse to show the 20-deg data, which fits perfectly in the high-energy region.) The poor fit in the evaporation region is sensitive to nuclear details – the predicted spectrum for ^{56}Fe fits the data! In all these measurements the deuteron cross section at the higher energies is about 1/10 of the proton cross section, though emerging deuterons cannot be predicted by the present cascade model. Deuterons and heavier particles are predicted to compete in the evaporation process, and Fig. 10 at 60 deg for the same target and energy includes comparisons for five particle types. For protons this case shows a less favorable comparison with calculation; the predicted cross section does not hold up well at energies over 40 MeV. In these figures the experimental data are shown as a smooth curve below the near-elastic region, though they were obtained in a thousand individual channels. In the smoothed regions the data have been shown to be statistically consistent with a smooth curve. Figures 11 and 12 show similar comparisons for 61-MeV protons on Bi. At 30 deg the calculation fits the proton cross sections only at high energies; at 60 deg there is no agreement. The failure of the model to predict a reasonably shaped spectrum for Bi may be related to the model's neglect of fission.

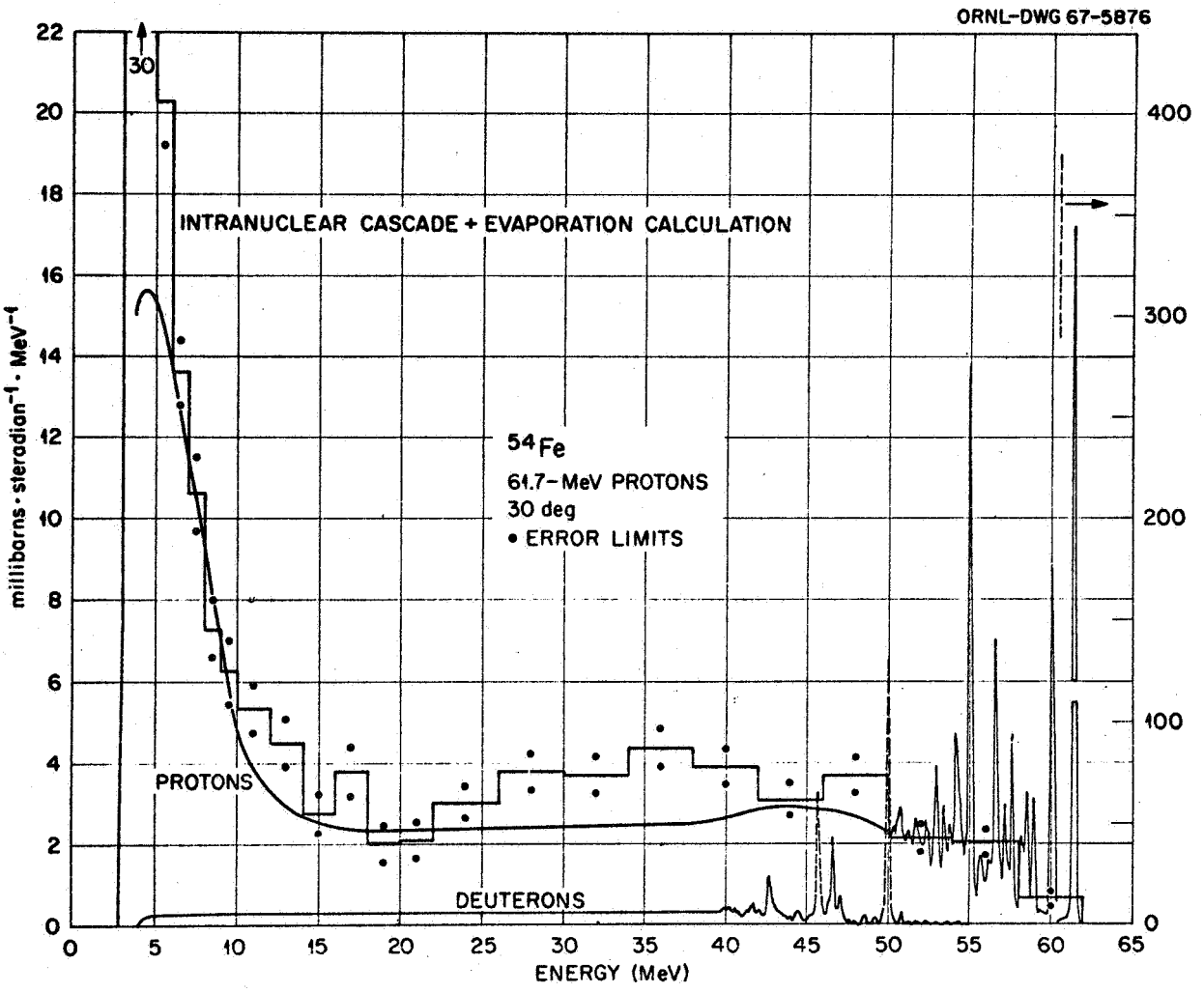

Fig. 9. Differential Cross Sections for Secondary Protons and Deuterons at 30 deg from 61-MeV Protons on ^{54}Fe. The experiment of Bertrand et al. is compared against intranuclear cascade-plus-evaporation calculations using the program of Bertini.

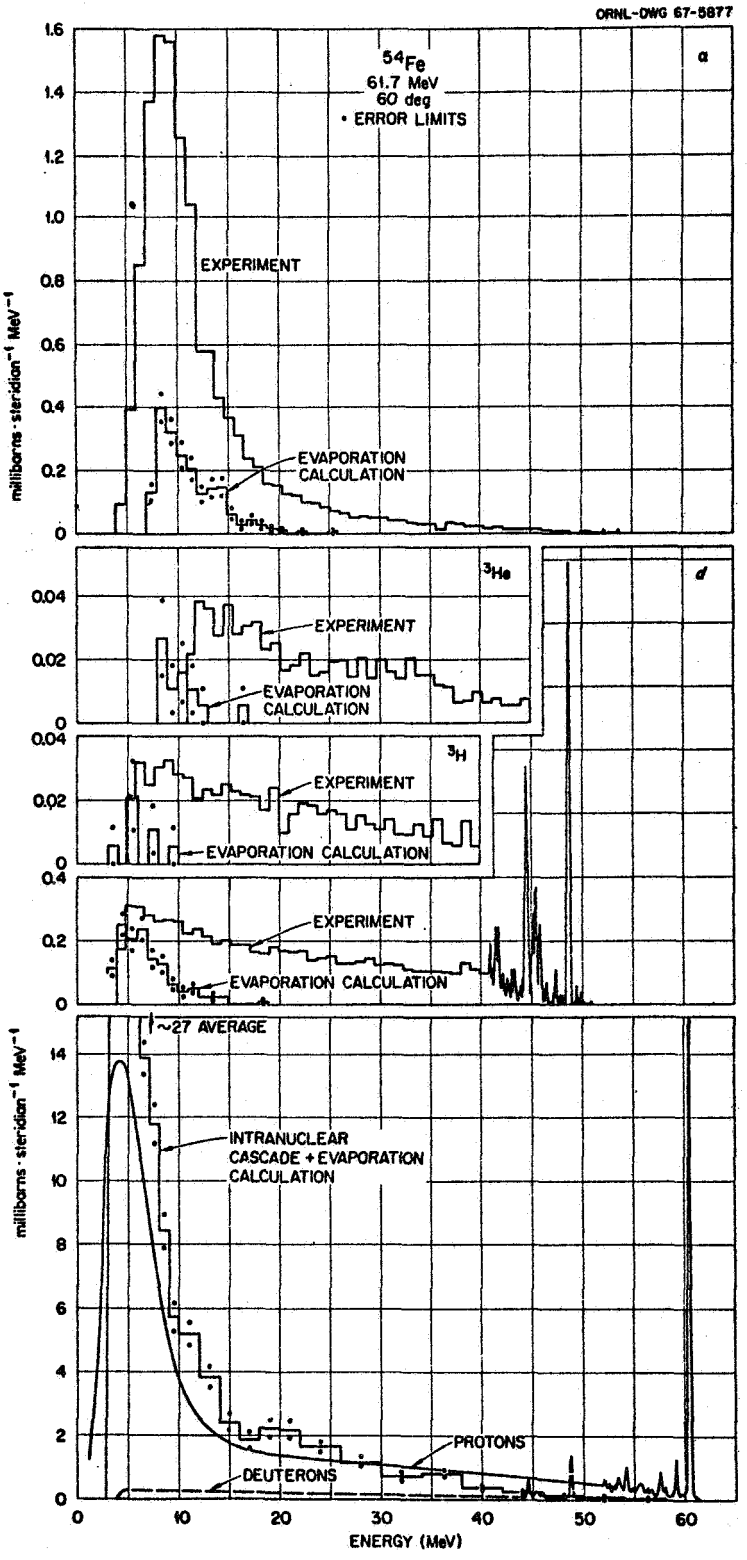

Fig. 10. Differential Cross Sections for Secondary p, d, t, ^{3}He, and ^{4}He Ions at 60 deg from 61-MeV Protons on ^{54}Fe Compared Against the Intranuclear Cascade-Plus-Evaporation Model.

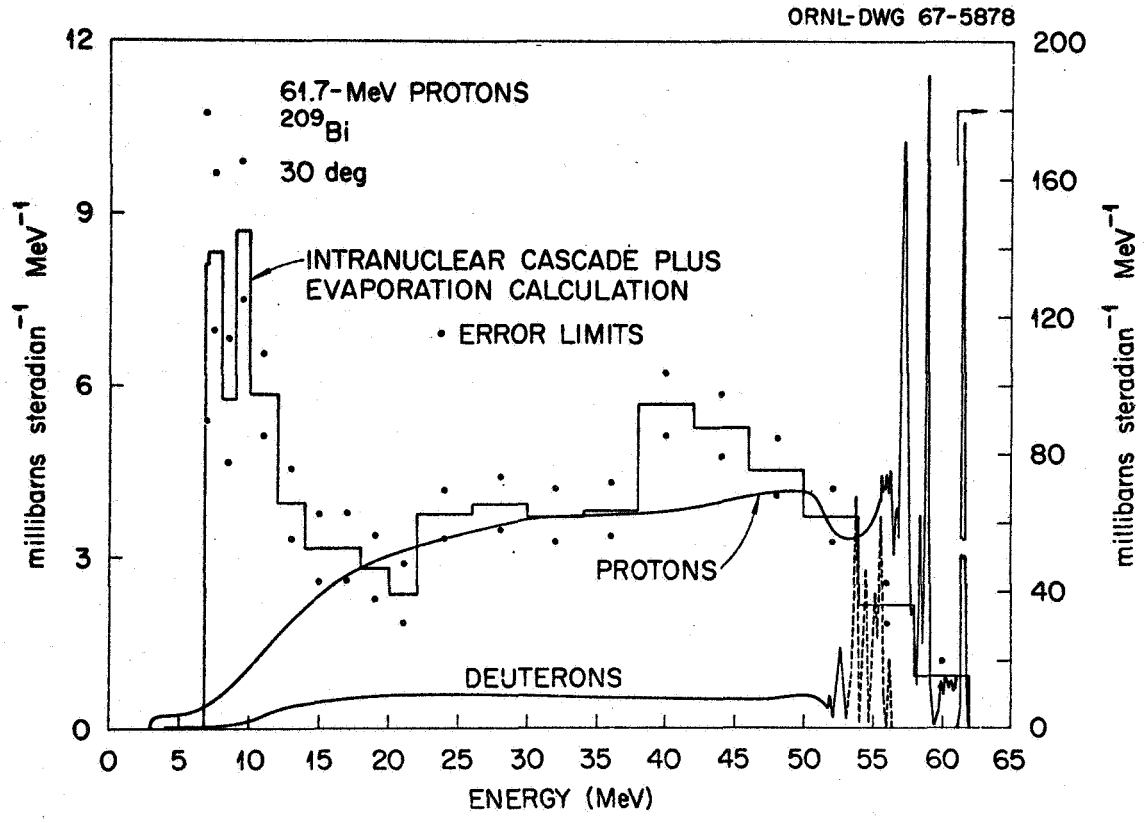

Fig. 11. Differential Cross Sections for Secondary Protons and Deuterons at 30 deg from 61-MeV Protons on ^{209}Bi Compared Against the Intranuclear Cascade-Plus-Evaporation Model.

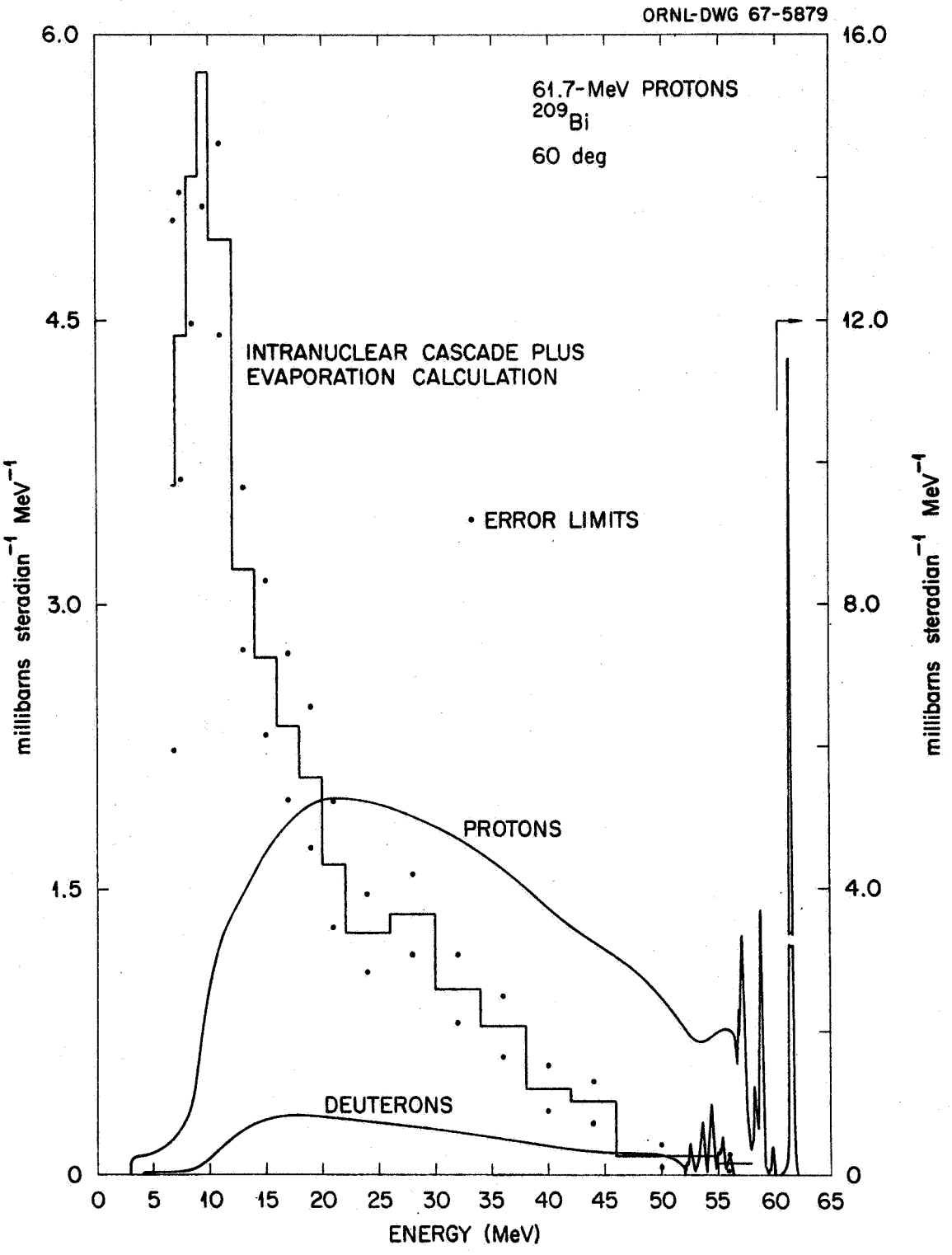

Fig. 12. Differential Cross Sections for Secondary Protons and Deuterons at 60 deg from 61-MeV Protons on ^{209}Be, Compared Against the Intranuclear Cascade-Plus-Evaporation Model.

When this work is completed we should have some picture of the validity of the cascade model for incident 60-MeV protons and emerging charged particles, with some few runs for incident 40-MeV protons and some for alpha particles. The 40-MeV proton data shows continuum regions similar to those at 60 MeV, but of course it becomes harder and harder to ignore the excitation of definite final states. Alpha particles do give substantial numbers of energetic secondary protons. Because of the importance of charged-particle reactions in dose calculations when the quality factor is given consideration, we will try to get data on C and O targets.

The lower energy limit for intranuclear cascade calculations can be pressed even more by looking at the new cross sections of Verbinski and Burrus[19] at 15 to 18 MeV for (p,n) reactions on several elements. The observed cross sections for elements as heavy as Fe show energy group structure and at the higher energies a definite angular distribution.

Figure 13 shows the cross sections $^{27}Al(p,n)$ integrated over solid angle. I have shown for each of two energies a comparison of experiment with a Monte Carlo evaporation theory of the Dostrovsky[8] type and with the cascade plus evaporation theory of Bertini. The evaporation-only calculations assume that all the incident energy is absorbed into a compound nucleus with an arbitrary 500-mb reaction cross section. Though imperfect, the Bertini estimate is the better though he is slightly shocked by our use of his program at these energies. Whether the agreement is satisfactory, and whether it can easily be improved upon, await further analysis. At least two problems other than the residual shape error arise in routinely applying the presently available cascade programs to this energy range. The calculated and observed spectra have high-energy end-points quite out of line when the (p,n) Q-value is far different from the zero estimate made in Bertini's

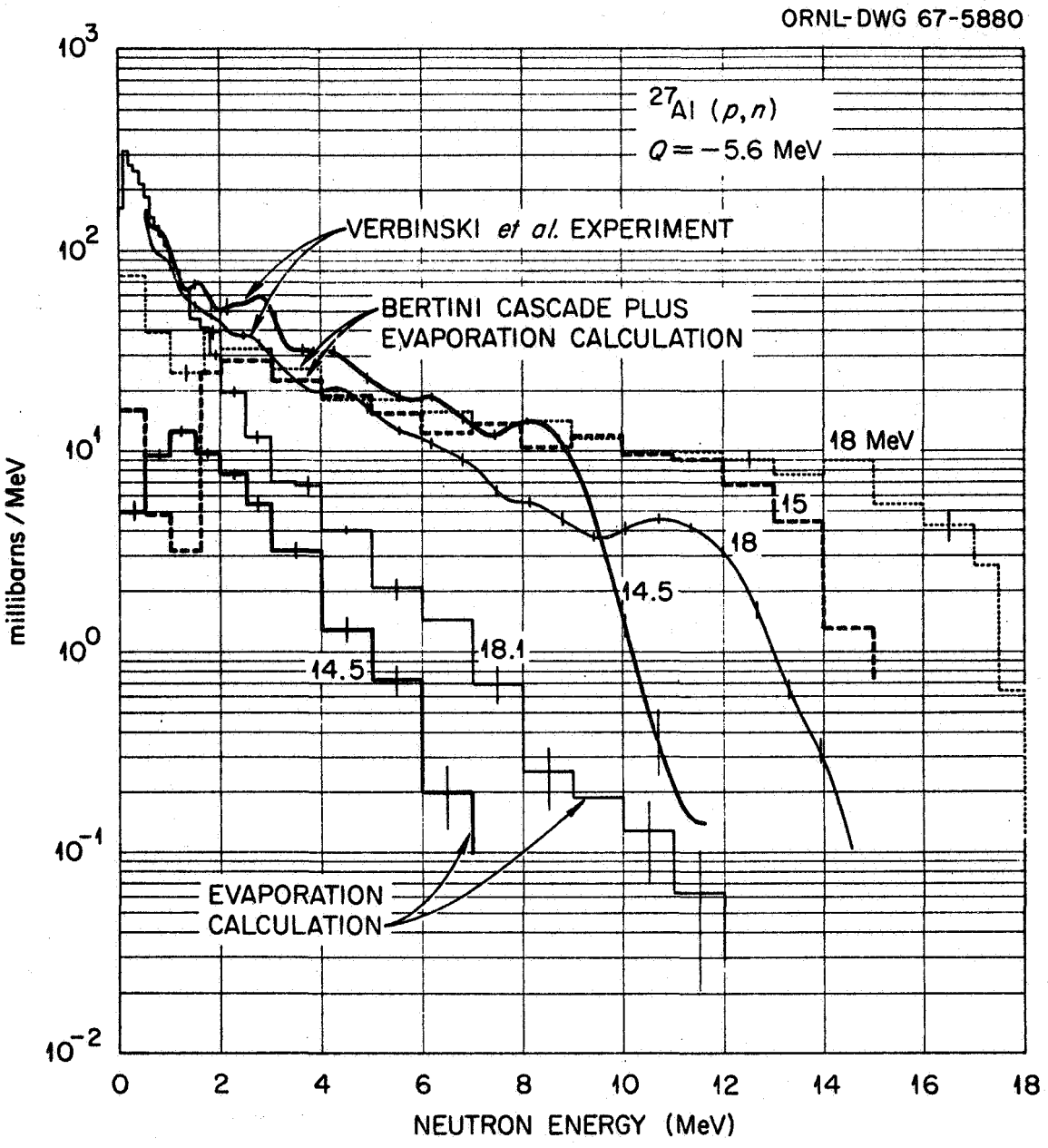

Fig. 13. Angle-Integrated Energy Spectra from 14.5- and 18-MeV Protons on Al. The experiment of Verbinski and Burrus is compared with cascade-plus-evaporation calculations and with "pure" evaporation calculations.

cascade program. This effect is apparent in Fig. 13. Also, as emphasized in Fig. 14 for Ta, the cutoff energy which customarily terminates the model cascade reactions produces a nonphysical kink in the predicted energy distributions. Lowering the cutoff from 6.6 to 2 MeV improved the behavior of the spectrum but markedly increased the computer running time. The evaporation-only model gives the same shape as the low-energy data shown for the 6.6-MeV cutoff, but 25% more intense if the same nonelastic cross section is used.

I have little to report on neutron production by alpha particles, except to observe that in the case of the $^{9}Be(\alpha,n)$ reaction the cross section is large, between 400 and 700 mb for alpha particles between 5 and 10 MeV, and the energy spectrum does not much resemble an evaporation spectrum. This integrated cross section is as large as the geometrical cross section of sulphur, and if it remains so large at higher energies it would imply that about 4% of the 60-MeV alpha particles stopping in a Be shield would produce neutrons. Figure 15 illustrates the angle-integrated neutron spectra obtained by Verbinski[20] for two incident energies, illustrating that even at low resolution there is definite character to the spectra. The angular distributions are also marked. It may always be necessary to take this type of data from experiment.

III. CROSS SECTIONS FOR SECONDARY GAMMA RAYS

Finally there is the problem of secondary gamma rays. As I indicated earlier, conclusions await the implications of the spectra that Zobel, Maienschein, and Scroggs[1] have obtained at incident energies from 14 to 160 MeV, and the developing information concerning the intensity of soft

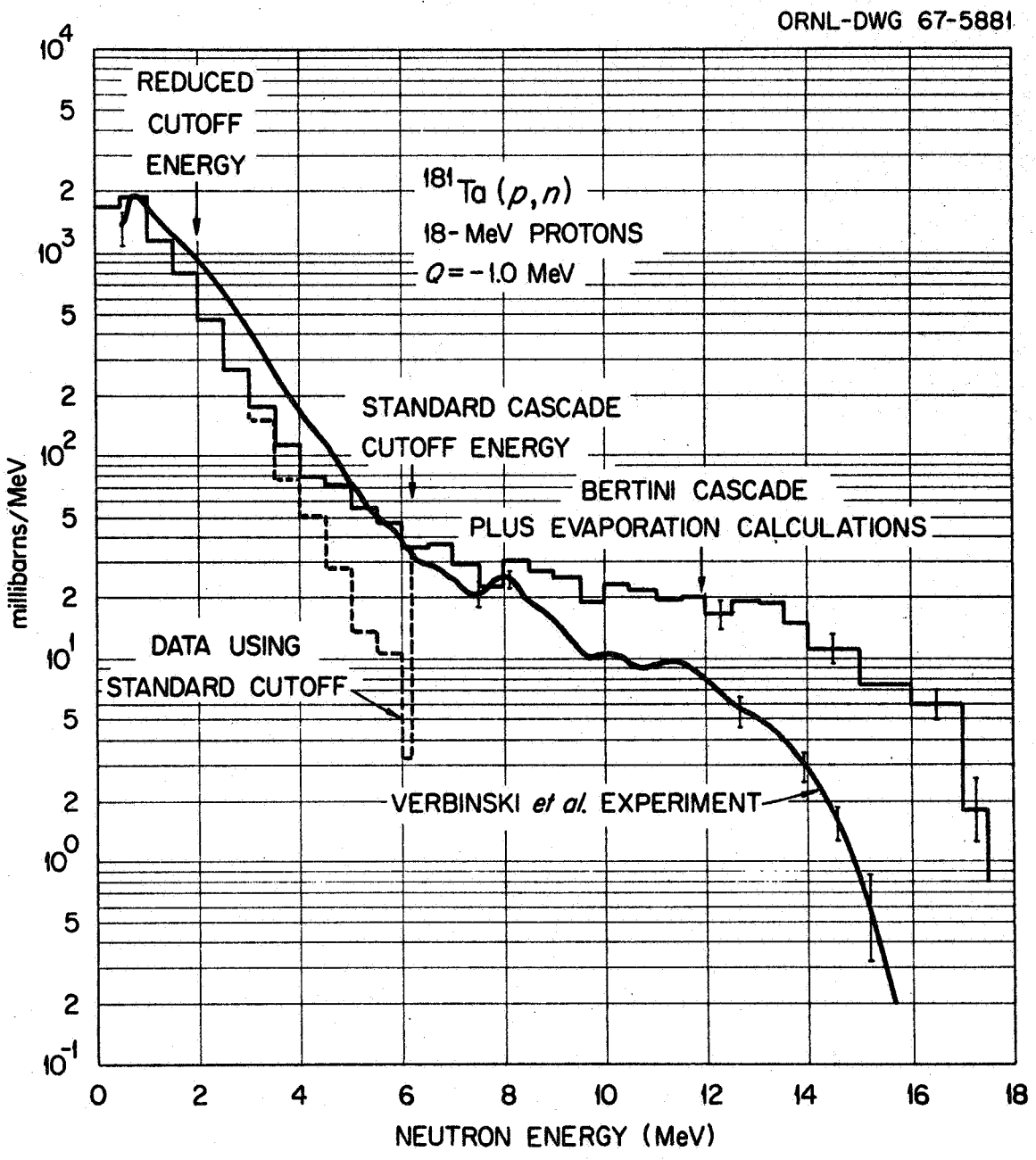

Fig. 14. Angle-Integrated Energy Spectra from 18-MeV Protons on ^{*181}Ta. The experiment of Verbinski and Burrus is compared with cascade-plus-evaporation calculations.

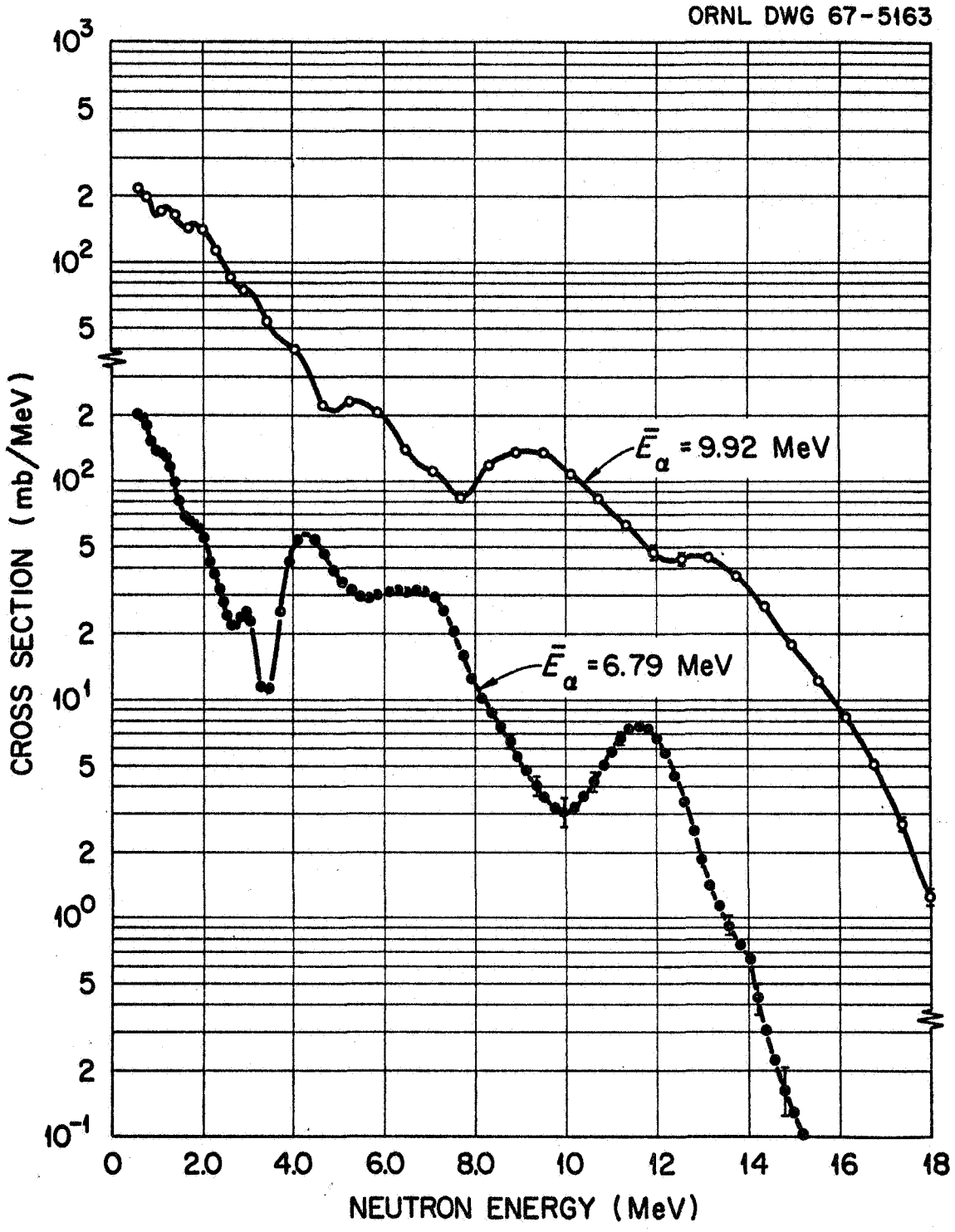

Fig. 15. Angle-Integrated Neutron Spectra from the $^9Be(\alpha,n)$ Reaction for 6.8- and 9.9-MeV Incident Alpha Particles. From the experiments of Verbinski.

flares. Figure 16, showing gamma rays from 33-MeV protons on H_2O, serves to remind us that such gamma rays are real.

IV. CONCLUSIONS

To summarize, I believe our course should be to use the cascade plus evaporation data, made widely available by Bertini et al., at even very low energies. We must however search for an effective way to join this system with a type of cross-section system more suitable for the lower energies. We must devise suitable cross-section estimators for incident helium ions and for secondary gamma rays.

Once the energies of incident particles become so low that their ranges are short compared to shield thicknesses and to the attenuation lengths of secondaries, precalculated secondary yields as a function of incident energy would be helpful to shield computations. The difficulties of spacecraft geometry should not inhibit ever-improving estimations of secondary effects based on the simplest geometries. Finally, in considering secondaries, soft flares must receive the main attention.

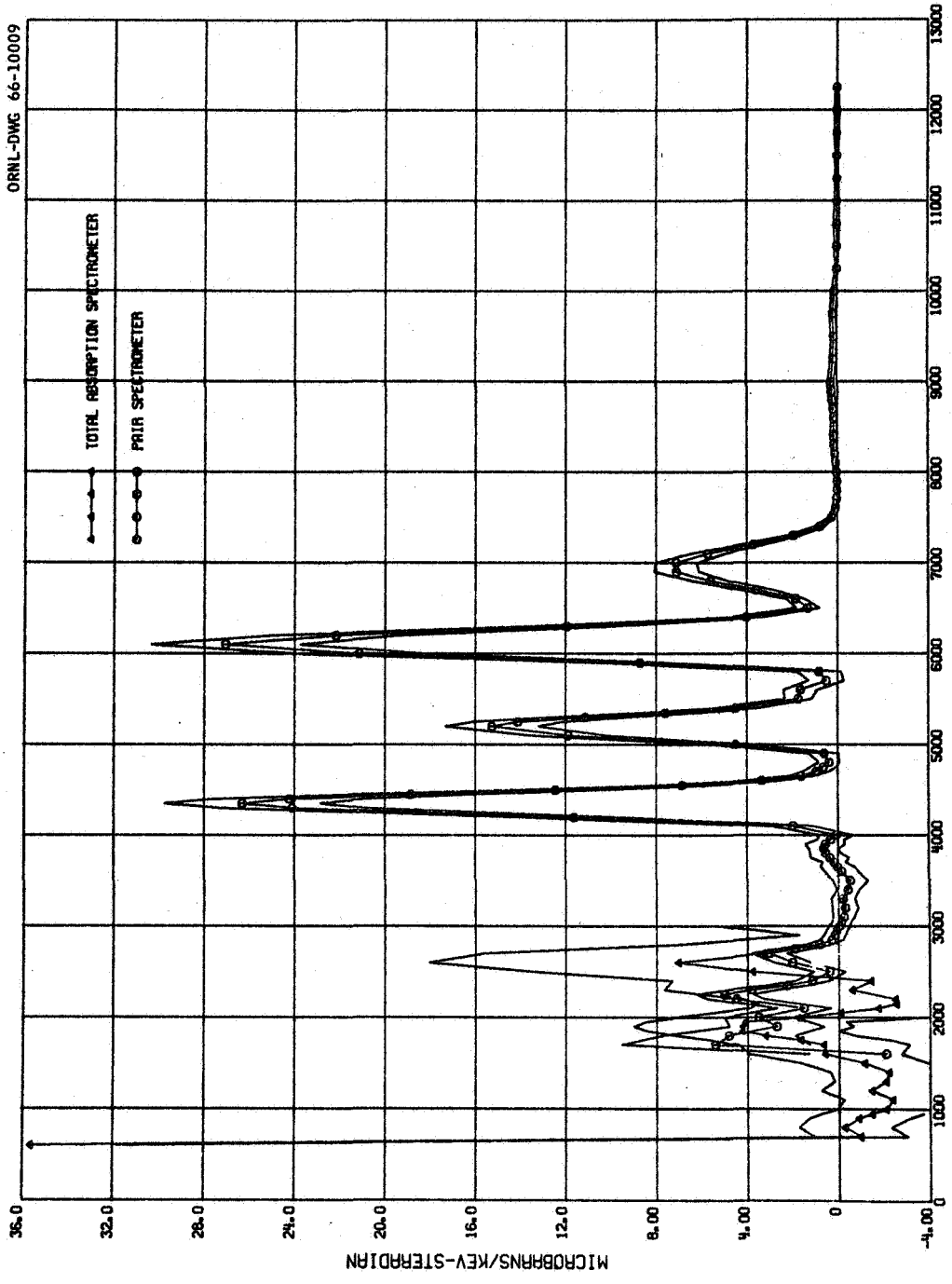

Fig. 16. Gamma-Ray Differential Cross Section Observed by Zobel and Maienschein at 135 deg from 33-MeV Protons on Water.

REFERENCES

1. W. ZOBEL, F. C. MAIENSCHEIN, and R. J. SCROGGS, "Spectra of Gamma Rays Produced by the Interaction of ~160-MeV Protons with Be, C, O, Al, Co, and Bi," ORNL-3506, Oak Ridge National Laboratory (April 1965); W. ZOBEL et al., "Secondary Gamma Rays from Proton Bombardment of ^{7}Li, Be, ^{11}B, C, O, Mg, Al, and Fe," in ORNL-3838, Vol. II, Oak Ridge National Laboratory (November 1965).

2. R. WALLACE, P. G. STEWARD, and C. SONDHAUS, "Primary- and Secondary-Proton Dose Rates in Spheres and Slabs of Tissue," Second Symposium on Protection Against Radiations in Space, NASA SP-71, Gatlinburg, Tennessee (October 1964).

3. Handbook of Mathematical Functions, M. Abramowitz and I. Stegren, eds., National Bureau of Standards Applied Mathematics Series 55 (1964); Formula 8.14.15.

4. N. METROPOLIS et al., "Monte Carlo Calculations on Intranuclear Cascades. I. Low-Energy Studies," Phys. Rev. 110, 185 (1958); "Monte Carlo Calculations on Intranuclear Cascades. II. High-Energy Studies and Pion Processes," Phys. Rev. 110, 204 (1958).

5. H. W. BERTINI, "Low-Energy Intranuclear Cascade Calculation," Phys. Rev. 131, 1801 (1963), with erratum Phys. Rev. 138, AB2 (1965); "Monte Carlo Calculations on the Intranuclear Cascades," ORKL-3383, Oak Ridge National Laboratory (April 23, 1963); "Description of Printed Output from Intranuclear Cascade Calculation," ORNL-3433, Oak Ridge National Laboratory (May 14, 1963).

6. R. G. ALSMILLER, JR., M. LEIMDORFER, and J. BARISH, "Analytic Representation of Nonelastic Cross Sections and Particle-Emission Spectra from Nucleon-Nucleus Collisions in the Energy Range 25 to 400 MeV," ORNL-4046, Oak Ridge National Laboratory (April 1967).

7. H. W. BERTINI, "Results from Low-Energy Intranuclear-Cascade Calculation," ORNL-TM-1225, Oak Ridge National Laboratory (September 1965).

8. I. DOSTROVSKY, Z. FRAENKEL, and G. FRIEDLANDER, "Monte Carlo Calculations of Nuclear Evaporation Processes. III. Applications to Low-Energy Reactions," Phys. Rev. 116, 683 (1959); I. DOSTROVSKY, Z. FRAENKEL, and L. WINSBERG, "Monte Carlo Calculations of Nuclear Evaporation Processes. IV. Spectra of Neutrons and Charged Particles from Nuclear Reactions," Phys. Rev. 118, 781 (1960).

9. N. S. WALL and P. R. ROOS, "Quasifree Scattering of 160-MeV Protons from Nuclei," Phys. Rev. 150, 811 (1966).

10. J. GENIN et al., "Protons, Deutons, Tritons, et Noyaux d'Hélium Démis par ^{197}Au sous l'Action de Protons de 154 MeV," J. Phys. Radium 22, 615 (1961); "Etude des Deutons et des Triton Emis lors du Bombardement de Noyaux de Carbone par des Protons de 155 MeV," J. Phys. Radium 21, 322 (1960).

11. R. W. PEELLE et al., "Differential Cross Sections for the Production of Protons in the Reactions of 160-MeV Protons on Complex Nuclei," ORNL-3887, Oak Ridge National Laboratory (September 1966).

12. C. BRUN et al., "Direct Interaction Protons Emitted from Ag and Au Targets Bombarded by 156 MeV and 91 MeV Protons," Nucl. Phys. A95, 337 (1967).

13. S. DAHLGREN et al., "A Study of the Large-Angle Emission of Charged Particle from Nuclei Bombarded by 186-MeV Protons," Arkiv Fysik 32, 510 (1964).

14. J. W. WACHTER, W. R. BURRUS, and W. A. GIBSON, "Neutron and Proton Spectra from Targets Bombarded by 160-MeV Protons," ORNL-TM-1781, Oak Ridge National Laboratory (1967).

15. P. H. BOWEN et al., "Neutrons Emitted at 0° from Nuclei Bombarded by 143-MeV Protons," Nucl. Phys. 30, 475 (1962).

16. H. W. BERTINI, "Intermediate-Energy Intranuclear-Cascade Calculation," Bulletin of the American Physical Society, 1967 Spring Meeting at Washington, D. C., April 24-27, 1967; also to be published in the Neutron Physics Division Annual Progress Report for period ending April 30, 1967, ORNL-4134, Oak Ridge National Laboratory.

17. L. S. AZHGIREY et. al., "Nuclear Interactions of 660-MeV Protons and the Momentum Distribution of Nucleons in Nuclei," Nucl. Phys. 13, 258 (1959).

18. F. E. BERTRAND et al., "The Mass and Energy Spectra of Charged Reaction Particles from Targets Bombarded by 60-MeV Protons," Neutron Physics Division Annual Progress Report for Period Ending April 30, 1967, ORNL-4134, Oak Ridge National Laboratory.

19. V. V. VERBINSKI, Oak Ridge National Laboratory, personal communication (May 1967).

20. V. V. VERBINSKI et al., "Neutrons from $^{9}Be(\alpha,n)$ Reactions at 6-10 MeV." Oak Ridge National Laboratory (to be published).

INTERNAL DISTRIBUTION

1-2. L. S. Abbott
3. F. S. Alsmiller
4. R. G. Alsmiller, Jr.
5. T. W. Armstrong
6. H. W. Bertini
7. F. E. Bertrand
8. W. R. Burrus
9. V. R. Cain
10. H. C. Claiborne
11. C. E. Clifford
12. W. A. Gibson
13. M. P. Guthrie
14. D. C. Irving
15. W. H. Jordan
16. T. A. Love
17. F. C. Maienschein
18. H. S. Moran
19-28. R. W. Peelle
29. R. T. Santoro
30. E. G. Silver
31. D. K. Trubey
32. V. V. Verbinski
33. J. W. Wachter
34. A. M. Weinberg
35. W. Zobel
36. G. Dessauer (consultant)
37. B. C. Diven (consultant)
38. M. H. Kalos (consultant)
39. L. V. Spencer (consultant)
40-41. Central Research Library
42. Document Reference Section
43-263. Laboratory Records Department
264. Laboratory Records ORNL RC
265. ORNL Patent Office

EXTERNAL DISTRIBUTION

266. P. B. Hemmig, Division of Reactor Development and Technology, U. S. Atomic Energy Commission, Washington, D. C. 20545
267. I. F. Zartman, Division of Reactor Development, U. S. Atomic Energy Commission, Washington, D. C. 20545
268-282. Division of Technical Information Extension (DTIE)
283. Division of Research and Development (ORO)